New Force Field for Molecular Simulation of Guanidinium-Based Ionic Liquids

Xiaomin Liu,[†,‡] Suojiang Zhang,*[,†] Guohui Zhou,[†,‡] Guangwen Wu,[§] Xiaoliang Yuan,[†,‡] and Xiaoqian Yao[†]

Research Laboratory of Green Chemistry and Technology, Institute of Process Engineering, Chinese Academy of Sciences, 100080 Beijing, China, Graduate University of Chinese Academy of Sciences, 100049 Beijing, China, and Center for Molecular Simulation, Swinburne University of Technology, Vic 3122, Australia

Received: February 8, 2006; In Final Form: April 13, 2006

An all-atom force field was proposed for a new class of room temperature ionic liquids (RTILs), *N*,*N*,*N*′,*N*′-tetramethylguanidinium (TMG) RTILs. The model is based on the AMBER force field with modifications on several parameters. The refinements include (1) fitting the vibration frequencies for obtaining force coefficients of bonds and angles against the data obtained by ab initio calculations and/or by experiments and (2) fitting the torsion energy profiles of dihedral angles for obtaining torsion parameters against the data obtained by ab initio calculations. To validate the force field, molecular dynamics (MD) simulations at different temperatures were performed for five kinds of RTILs, where TMG acts as a cation and formate, lactate, perchlorate, trifluoroacetate, and trifluoromethylsulfonate act as anions. The predicted densities were in good agreement with the experimental data. Radial distribution functions (RDFs) and spatial distribution functions (SDFs) were investigated to depict the microscopic structures of the RTILs.

1. Introduction

Recently, room temperature ionic liquids (RTILs) have prompted a significant amount of research.[1] The most attractive property of RTILs is their use as environmentally benign solvents that can replace organic compounds in chemical reactions,[2−4] separation, fractionation,[5,6] and so forth. As a designable solvent, a number of functional ionic liquids have been synthesized. However, the microstructures and interactions for most of the RTILs have not been clearly understood yet. Molecular simulation provides an effective way for understanding the microstrcutures and interactions of ionic pairs. Many physical properties of RTILs have been studied by computer simulation, such as molar volumes, volume expansivity, isothermal compressibility, self-diffusivities, cation−anion exchange rates, and rotational dynamics.[1,7,8]

It is well-known that cations such as ammonium, phosphonium, sulfonium, pyridinium, pyrrolidinium, and imidazolium can form room temperature ionic liquids with a variety of anions,[9−13] but most of the research is based on the RTILs formed by 1-alkyl-3-methyl-imidazolium cation. Recently, the *N*,*N*,*N*′,*N*′-tetramethylguanidinium (TMG)-based ionic liquids have attracted much attention due to their wide applications. It is reported that these RTILs can be used in the absorption of acid gases, such as SO_2, CO_2, and so on,[14] which causes environmental problems. The guanidinium-based RTILs, due to their exceptional stability at high temperature, can be synthesized directly by neutralization of acids and guanidinium salts which are widely used as phase transfer catalysts. The positive charge in the guanidinium salts is delocalized over one carbon and three nitrogen atoms, which gives them a high degree of thermal stability compared to tetraalkylammonium salts.[15] However, the force field for guanidinium-based ionic liquids has not been developed.

In this work, a new force field based on AMBER has been exploited for five kinds of RTILs, where TMG acts as a cation and formate (F), lactate (L), perchlorate (P), trifluoroacetate (T), and trifluoromethylsulfonate (Tf) acts as anions, respectively. The refinement for the force field includes two aspects: (1) The force coefficients of the bond and angle were adjusted by fitting the vibrational frequency data from ab initio calculations. (2) The parameters for torsions were obtained by fitting the torsion energy profiles of dihedral angles. Molecular dynamics simulations were performed to test the accuracy of the force field. The simulation results are comparable to experimental data.

2. Force Field Development

In this work, we use a standard molecular mechanics force field with the functional form

$$E(r^N) = \sum_{\text{bonds}} K_r(r - r_0)^2 + \sum_{\text{angles}} K_\theta(\theta - \theta_0)^2 + \sum_{\text{torsions}} \frac{K_\phi}{2}(1 + \cos(n\phi - \gamma)) + \sum_{i=1}^{N}\sum_{j=i+1}^{N}\left\{4\epsilon_{ij}\left[\left(\frac{\sigma_{ij}}{r_{ij}}\right)^{12} - \left(\frac{\sigma_{ij}}{r_{ij}}\right)^{6}\right] + \frac{q_i q_j}{r_{ij}}\right\} \quad (1)$$

The first three terms in eq 1 represent the bonded interactions: bonds, angles, and torsions. The nonbonded interactions include van der Waals (VDW, in the Lennard-Jones (LJ) 6−12 form) and Coulombic interactions of atom-centered point charges. Electrostatic and VDW interactions are calculated for the atoms in different molecules or in the same molecule separated by

* To whom correspondence should be addressed. E-mail: sjzhang@home.ipe.ac.cn.
† Institute of Process Engineering, Chinese Academy of Sciences.
‡ Graduate University of Chinese Academy of Sciences.
§ Swinburne University of Technology.

10.1021/jp060834p CCC: $33.50
Published on Web 06/01/2006

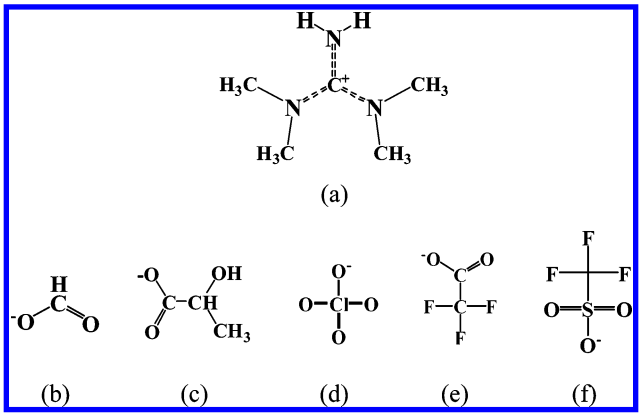

Figure 1. Structures of the cation and anions: (a) TMG; (b) F; (c) L; (d) P; (e) T; (f) Tf.

more than three bonds. The nonbonded interactions separated by exactly three bonds (1−4 interactions) are reduced by a scale factor, which is optimized as 1/2 for VDW and 1/1.2 for electrostatic interactions.[16] The LJ parameters for unlike atoms are obtained from the Lorentz−Berthelot (LB) combining rule.[17]

The force field parameters are modified as follows:

(1) Assign the atom type based on the AMBER99 force field.

(2) Perform a quantum mechanics (QM) calculation for the cation and anion, respectively, and obtain the optimized molecular geometry and the equilibrium bond lengths and angles.

(3) Allocate charge to each atom center by fitting the ab initio electrostatic potential (ESP).

(4) Adjust bond and angle force constants to fit the vibration frequency data.

(5) Adjust torsion parameters by fitting the torsion energy profiles.

(6) Repeat steps 4 and 5, until the deviations between the two sets of parameters are small enough.

(7) Validate the force field through molecular dynamics simulation.

2.1. Atom Types Assignment. The assignments of most atom types of the TMG cation are straightforward, because the atom types are similar to arginine defined in AMBER. The structure and assignment of the atom types of both the cation and anions are shown in Figures 1 and 2, respectively. The VDW parameters are directly taken from AMBER99 (refer to Table 1). The force field parameters for the trifluoromethylsulfonic acid group (Tf) obtained from ref 18 and adjusted in this work are both listed in Table 1.

2.2. Geometries of Isolated Ions. The isolated ions were optimized using the Gaussian 03 package at the HF/6-31+G-(d) level. The initial cation and anion charges were set at +1 and −1, respectively. The minimized structure was used to set equilibrium bond lengths (r_0) and angles (θ_0). Once the optimized geometries were obtained, the vibration frequencies were checked to ensure no negative frequencies existed and verify the ion energy of a true minimum. The minimum conformers here are in agreement with the experimental data.[19] The most notable characteristic of the cation is that the guanidine group is planar, which has been proved by the X-ray diffraction data.[19]

2.3. Force Constants of Bonds and Angles. The force constants were adjusted by fitting vibration frequencies calculated by molecular mechanics (MM) to the QM frequencies.[20] In this work, the vibration frequencies and the corresponding vibration modes of a single ion were obtained by MM calculation with the TINKER package.[17,21] Because the number of peaks in IR frequencies is far less than the quantity of freedom degree ($3N - 6$), the force constants K_r and K_θ were determined by performing a vibration analysis on the optimized ionic pairs with Gaussian 03 and adjusted according to the experimental

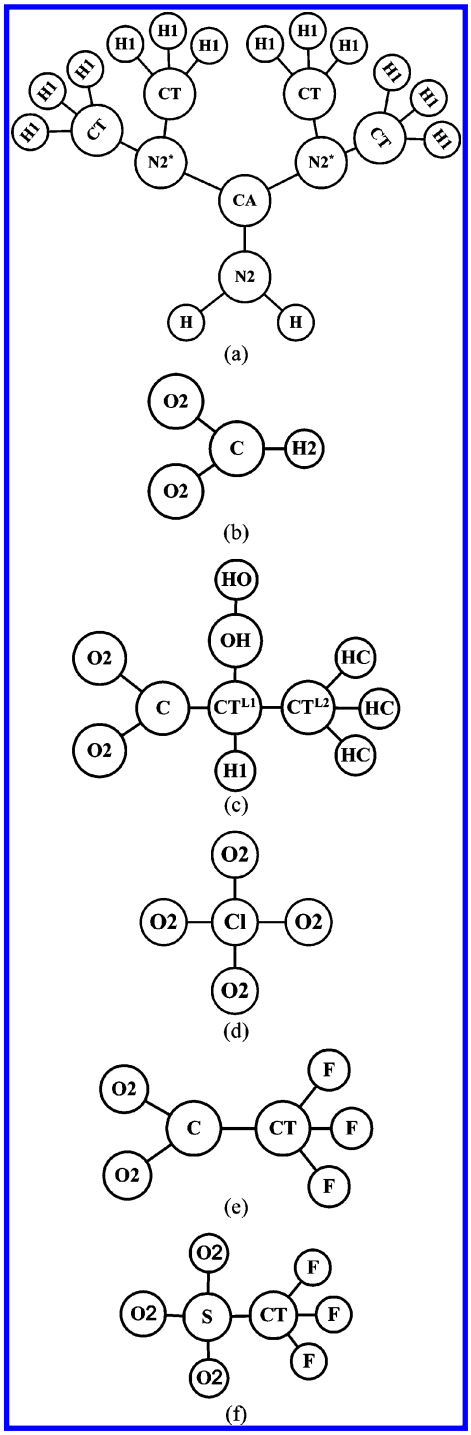

Figure 2. Assignment of the atom types for the cation and anions: (a) TMG; (b) F; (c) L; (d) P; (e) T; (f) Tf. The nomenclature of the atoms is adopted from AMBER99 as follows: CT, sp^3 aliphatic C; CA, any aromatic sp^2 C and Cϵ of argenine; C, sp^2 C in a carbonyl group; N2, sp^2 N of aromatic amines and guanidinium ions; H1, H attached to an aliphatic carbon with one electron withdrawing substituent; H2, H attached to an aliphatic carbon with two electron withdrawing substituents; H, H bonded to nitrogen atoms; HC, H attached to an aliphatic carbon without any electron withdrawing substituents; HO, H in a hydroxyl group; O2, sp^2 O in anionic acids; OH, O in a hydroxyl group; Cl, chlorine; F, fluorine; S, S in a disulfide linkage.

TABLE 1: Force Field Parameters for Guanidinium-Based RTILs[a]

Nonbonded Parameters (the VDW and Coulombic Interaction Parameters)

atom	ϵ_{ij} (kJ/mol)	σ_{ij} (Å)	q_i (e)
	TMG		
CA	0.3598	3.400	0.1696
N2	0.7113	3.250	−0.6235
N2*	0.7113	3.250	0.0304
CT	0.4577	3.400	−0.1300
H1	0.0657	2.472	0.0947
H	0.0657	1.069	0.3745
	F		
O2	0.8786	2.960	−0.8440
C	0.3598	3.400	0.9092
H2	0.0657	2.293	−0.2212
	L		
O2	0.8786	2.960	−0.8030
C	0.3598	3.400	0.7595
CT^{L1}	0.4577	3.400	0.4640
CT^{L2}	0.4577	3.400	−0.0723
OH	0.8803	3.067	−0.8072
HO	0.0000	0.000	0.3995
H1	0.0657	2.472	−0.0915
HC	0.0657	2.650	0.0154
	P		
O2	0.8786	2.960	−0.5203
Cl	1.1088	3.471	1.0813
	T		
O2	0.8786	2.960	−0.7808
C	0.3598	3.400	0.8309
CT	0.4577	3.400	0.5006
F	0.2552	3.118	−0.2567
	Tf		
CT	0.4577	3.400	0.2773
F	0.2552	3.118	−0.1650
S	1.0460	3.564	1.1185
O2	0.8786	2.960	−0.6336
	Tf^{18}		
C	0.2761	3.500	0.2719
F	0.2218	2.950	−0.1638
S	1.0406	3.550	1.0460
O	0.8786	2.960	−0.6829

Bonded Parameters 1

bond	r_0 (Å)	K_r (kJ/mol)	source
	TMG		
CA−N2	1.332/1.3198[b]	1464.40	this work
CA−N2*	1.330/1.3447[b,c]	1464.40	this work
N2*−CT	1.467/1.461[b,d]	1255.20	this work
CT−H1	1.085	1464.40	this work
N2−H	0.995	2050.16	this work
	F		
C−H2	1.118	1573.18	this work
C−O2	1.234	2719.60	this work
	L		
O2−C	1.237	2744.70	AMBER
$C-CT^{L1}$	1.552	1297.04	this work
$CT^{L1}-CT^{L2}$	1.524	1297.04	AMBER
CT^{L1}−OH	1.407	1338.88	AMBER
CT^{L1}−H1	1.088	1317.96	this work
OH−HO	0.957	2112.92	this work
CT^{L2}−HC	1.088	1389.09	this work
	P		
Cl−O2	1.452	1799.12	this work
	T		
C−CT	1.568	1087.84	this work
C−O2	1.223	2322.12	this work
CT−F	1.334	1004.16	this work
	Tf		
CT−F	1.324	1004.16	this work
CT−S	1.832	1087.84	this work
O2−S	1.443	2301.20	this work
	Tf^{18}		
C−F	1.323	1848.50	ref 18
C−S	1.818	985.00	ref 18
O−S	1.442	2665.50	ref 18

TABLE 1. (Continued)

Bonded Parameters 2

angle	θ_0 (deg)	K_θ (kJ/mol)	source
	TMG		
N2−CA−N2*	119.00/120.22[b,e]	309.62	this work
N2*−CA−N2*	121.90/119.01[b]	292.88	AMBER
CA−N2−H	121.50	209.20	AMBER
H−N2−H	117.00	108.78	this work
CA−N2*−CT	121.90/121.27[b,f]	209.20	AMBER
CT−N2*−CT	115.00/115.34[b,g]	292.88	this work
N2*−CT−H1	110.00	217.57	this work
H1−CT−H1	108.90	154.81	this work
	F		
H2−C−O2	114.70	334.72	this work
O2−C−O2	130.50	502.08	this work
	L		
O2−C−O2	129.40	376.56	this work
O2−C−CT^{L1}	115.30	251.04	this work
C−CT^{L1}−CT^{L2}	111.80	271.96	this work
C−CT^{L1}−OH	110.50	209.20	this work
C−CT^{L1}−H1	107.20	209.20	AMBER
CT^{L2}−CT^{L1}−OH	109.90	209.20	AMBER
CT^{L2}−CT^{L1}−H1	108.80	209.20	AMBER
OH−CT^{L1}−H1	108.60	167.36	this work
CT^{L1}−CT^{L2}−HC	110.30	221.75	this work
HC−CT^{L2}−HC	108.60	121.34	this work
CT^{L1}−OH−HO	103.70	209.20	this work
	P		
O2−Cl−O2	109.50	460.24	this work
	T		
CT−C−O2	113.60	167.36	this work
O2−C−O2	132.80	439.32	this work
C−CT−F	112.80	376.56	this work
F−CT−F	106.00	585.76	this work
	Tf		
F−CT−F	107.08	502.08	this work
F−CT−S	111.77	292.88	this work
CT−S−O2	102.59	418.40	this work
O2−S−O2	115.39	523.00	this work
	Tf[18]		
F−C−F	107.10	390.50	ref 18
F−C−S	111.80	347.00	ref 18
C−S−O	102.60	435.00	ref 18
O−S−O	115.30	484.50	ref 18

Bonded Parameters 3

torsion	γ (deg)	K_ϕ (kJ/mol)	n	source
	TMG			
N2*−CA−N2−H	180.00	7.812	2	this work
N2−CA−N2*−CT	180.00	11.715	2	this work
N2*−CA−N2*−CT	180.00	11.715	2	this work
CA−N2*−CT−H1	0.00	0.000	3	this work
CT−N2*−CT−H1	0.00	0.686	3	this work
	L			
O2−C−CT^{L1}−CT^{L2}	0.00	0.837	2	this work
O2−C−CT^{L1}−OH	0.00	−0.418	2	this work
O2−C−CT^{L1}−H1	0.00	2.092	2	this work
C−CT^{L1}−CT^{L2}−HC	0.00	0.653	3	AMBER
OH−CT^{L1}−CT^{L2}−HC	0.00	0.653	3	AMBER
H1−CT^{L1}−CT^{L2}−HC	0.00	0.653	3	AMBER
C−CT^{L1}−OH−HO	0.00	0.000	3	this work
CT^{L2}−CT^{L1}−OH−HO	0.00	0.105	1	AMBER
H1−CT^{L1}−OH−HO	0.00	0.699	3	AMBER
	T			
O2−C−CT−F	0.00	0.209	3	this work
	Tf			
F−CT−S−O2	0.00	0.954	3	this work
	Tf[18]			

torsion	V1 (kJ/mol)	V2 (kJ/mol)	V3 (kJ/mol)	source
F−C−S−O	0.00	0.000	1.451	ref 18

[a] N2*, nitrogen connected with two methyls; N2, nitrogen in the amino-group terminal; CT^{L1}, carbon connected with hydroxyl in lactate anion; CT^{L2}, carbon of the methyl atom in lactate anion. [b] The experimental structure data were taken from ref 19. [c] The experimental data for the two CA−N2* bonds are 1.3447 and 1.3451 Å, respectively. [d] The experimental data are 1.461, 1.458, 1.466, and 1.455 Å. [e] The experimental data are 120.22 and 120.78°. [f] The experimental data are 121.27, 121.02, 121.53, and 120.91°. [g] The experimental data are 115.34 and 114.50°.

TABLE 2: Vibration Frequency Values (in cm^{-1}) from Experiment, QM, and MM

exp	QM	MM	vibration form	exp	QM	MM	vibration form
			Cation				
	103	81	complex bend	1120	1317	1242	N−C str
	116	87	$C(CH_3)-N-C(CH_3)$ bend	1374	1429	1428	CH_3 bend
	150	145	CH_3 tor		1433	1419	CH_3 bend
	185	176	complex bend		1439	1433	CH_3 bend
	192	184	CH_3 tor		1450	1445	CH_3 bend
	202	185	CH_3 tor	1452	1467	1448	$H-C(CH_3)-H$ bend
	233	206	CH_3 tor		1475	1435	$H-C(CH_3)-H$ bend
	258	269	CH_3 tor		1475	1453	$H-C(CH_3)-H$ bend
	271	304	complex bend		1478	1453	$H-C(CH_3)-H$ bend
	334	369	H−N−H bend		1486	1455	$H-C(CH_3)-H$ bend
	362	372	$C(CH_3)-N-C(CH_3)$ bend		1486	1524	$H-C(CH_3)-H$ bend
	372	415	NH_2 bend		1494	1572	$H-C(CH_3)-H$ bend
	426	449	NH_2 bend		1494	1586	$H-C(CH_3)-H$ bend
	494	513	NH_2 bend		1546	1594	N−C str
	529	510	NH_2 bend		1603	1607	N−C−N bend
	536	480	NH_2 bend	1606	1655	1655	N−H bend
	694	608	$N-C(CH_3)$ str	2934	2899	2884	C−H str
	726	543	C(mid) o/p bend		2899	2885	C−H str
	837	816	NH_2 bend		2919	2914	C−H str
	1031	943	CH_3 bend		2922	2914	C−H str
	1045	1014	NH_2 bend	2970	2978	2991	C−H str
	1057	1017	CH_3 bend		2978	2991	C−H str
	1068	1038	NH_2 bend		2982	3021	C−H str
	1109	1039	CH_3 bend		2982	3021	C−H str
	1110	1065	CH_3 bend		3009	2992	C−H str
	1142	1094	CH_3 bend		3009	2993	C−H str
	1142	1095	CH_3 bend		3028	3024	C−H str
	1194	1189	complex bend		3029	3024	C−H str
1093	1226	1137	complex bend		3453	3455	N−H str
	1261	1222	complex bend		3559	3568	N−H str
			Anion: Lactate Anion				
	68	62	complex bend		1240	1250	H−O−C bend
	228	239	CH_3 tor		1342	1300	H−C(mid)−C bend
	253	259	complex bend		1354	1325	H−O−C bend
	339	312	complex bend	1374	1391	1513	CH_3 bend
	407	354	O−C(mid)−C bend		1424	1363	H−O−C bend
	511	556	O−C−C(mid) bend	1452	1466	1377	$H-C-H(CH_3)$ bend
	571	454	O−H o/p bend		1474	1593	$H-C-H(CH_3)$ bend
	632	597	O−H o/p bend	1571	1659	1818	O−C−O bend
	768	705	$H-C(CH_3)-C$ bend		2856	2834	C(mid)−H str
	825	826	$H-C(CH_3)-C$ bend	2934	2866	2842	C−H str
	910	931	$H-C(CH_3)-C$ bend	2970	2908	2943	C−H str
	1028	1015	$H-C(CH_3)-C$ bend		2951	2945	C−H str
	1093	1069	$H-C(CH_3)-C$ bend	3203	3537	3532	O−H str
1036	1135	1085	$H-C(CH_3)-C$ bend				

data later. As the Hartree−Fock (HF) method overestimates the frequencies by approximately 10%,[22] a scaling factor of 0.9 is applied for HF calculations.[16] Comparison of the vibration modes for MM and QM was conducted manually until preferred force constant parameters were achieved. Taking TMGL as an example, the vibration frequency values obtained from experiment, QM at the HF/6-31+G(d) level, and MM are listed in Table 2.

2.4. Torsion Energy Barriers. The default torsion parameters are developed, including the ones related to the atom F. In this work, the ab initio torsion energy profiles were obtained at the MP2/6-31+G(d)//HF/6-31+G(d) level. The scans of energy profiles were started from the minimum, and the dihedral angle considered varied in a step of 10°. The final conformers from Gaussian 03 were used directly for molecular mechanics energy calculation in the Tinker module. The energy barrier fittings of N2*−CA−N2−CT and N2−CA−N2*−CT for the TMG cation are expressed in Figure 3.

2.5. Atom Charges. The atom charges are the most significant parts of force field parameters for ionic liquid systems. The mulliken charges, electrostatic potential (ESP) charges, and restraint electrostatic potential (RESP) charges have been compared, and the last one proved to be very efficient and successful for a variety of systems.[23−27] In this work, the one-conformation, two-step RESP method was used to derive the atom charges by fitting the electrostatic potential generated from QM calculations at the B3LYP/6-31+G(d) level. The RESP atom charges are listed in Table 1. The dipole moments of cation and anion calculated by the QM method and the RESP method are presented in Table 3. It can be seen that the differences between the two methods are very little.

2.6. Interaction Energies of Ion Pairs. The interaction energies were calculated by both MM and QM at the MP2/6-31+G(d)//HF/6-31G+(d) level. As reported, the QM calculation for ionic pair energy is dependent on the method and the basis sets.[7] For example, the interaction energies are −368.24 and −424.36 kJ mol^{-1} for TMGL at the B3LYP/6-31+G(d) level and the MP2/6-31+G(d)//HF/6-31G+(d) level, respectively. The results are listed in Table 4.

3. Simulations Details

Molecular dynamics (MD) simulations for the five RTILs were performed with the standard periodical boundary conditions

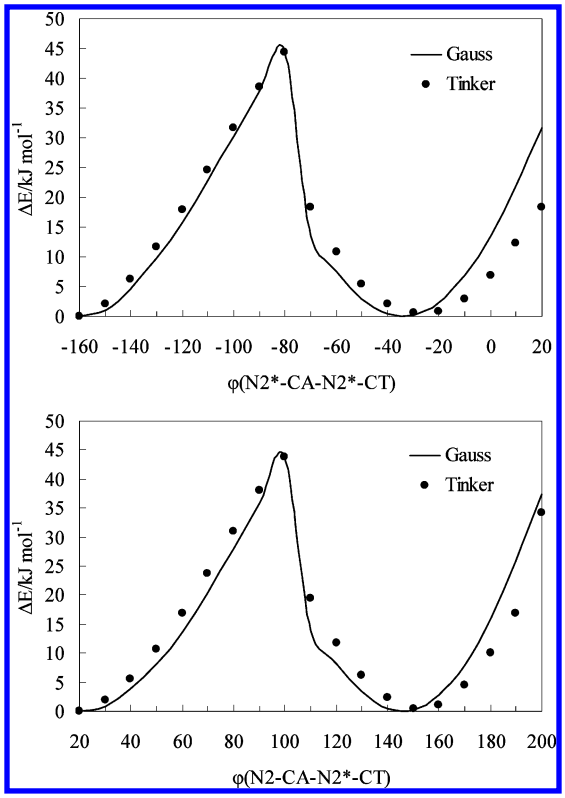

Figure 3. Energy barrier fittings of N2*−CA−N2*−CT and N2−CA−N2*−CT for TMG.

TABLE 3: Dipole Moments from the QM and Reproduced by the RESP Charges

ion	QM	RESP
TMG	1.4255	1.4750
F	1.4950	1.5079
L	4.2221	4.1224
P	0.0000	0.0000
T	4.8843	4.7832
Tf	4.1808	4.1420

TABLE 4: Ionic Pair Energy Calculated by QM and MM

RTIL	calculation method	energy (kJ/mol)
TMGF	QM	−448.04
	MM	−477.94
TMGL	QM	−424.36
	MM	−453.78
TMGP	QM	−382.11
	MM	−362.23
TMGT	QM	−436.29
	MM	−421.80
TMGTf	QM	−369.28
	MM	−393.70
	MM[a]	−483.23

[a] Result is based on the force field in the literature.[18]

using the M.DynaMix package.[28] Each system contained 256 ion pairs. A 2/0.2 fs multiple time-step algorithm was adopted. The intramolecule forces were cut off at 15 Å, while the long range forces including LJ and Coulombic interactions were cut off at half of the simulation boxes, and Ewald summation was implemented for the latter. All simulations started from a face-centered cubic (fcc) lattice with a low density of 0.2 g/cm^3. After the system was relaxed in the NVE ensemble for a few MD steps to remove the possible overlapping in the initial configuration,[17] the Nose−Hoover [29] NPT ensemble was adopted with coupling constants of 700 and 100 fs, and the system density gradually increased to a reasonable value. The system equilibrated for at least 400 ps, making sure the system

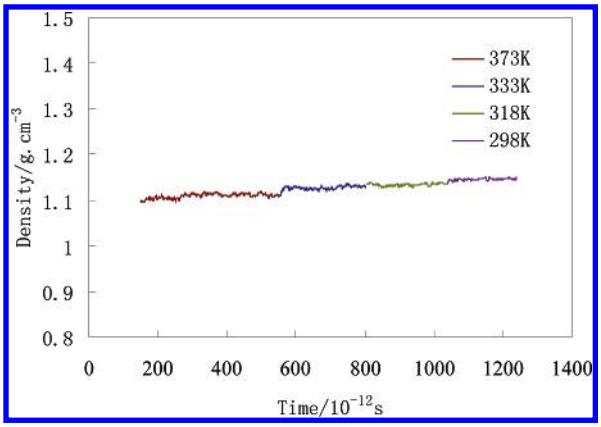

Figure 4. Evolution of density for TMGL during the simulation run.

TABLE 5: Intermolecular Interactions for the Guanidinium-Based RTILs at 373 K

RTIL		electrostatic interactions (kJ/mol)	Lennard-Jones interactions (kJ/mol)
TMGF	cation−cation	4564.79	−38.55
	cation−anion	−9575.13	−17.11
	anion−anion	4501.17	−2.66
	total	−509.17	−58.32
TMGL	cation−cation	3433.94	−26.40
	cation−anion	−7315.69	−37.98
	anion−anion	3401.80	−8.87
	total	−491.88	−73.28
TMGP	cation−cation	3958.99	−30.58
	cation−anion	−8325.11	−48.70
	anion−anion	3916.44	−6.87
	total	−449.68	−86.15
TMGT	cation−cation	3951.41	−26.55
	cation−anion	−8331.12	−32.74
	anion−anion	3914.63	−6.59
	total	−465.08	−65.88
TMGTf	cation−cation	3719.32	−23.37
	cation−anion	−7853.66	−48.59
	anion−anion	3691.60	−9.35
	total	−442.74	−81.31

configuration was stable. Each production phase lasted for 100 ps at 373, 333, 318, and 298 K under 1 atm. Trajectories were dumped in an interval of 10 fs for further analysis. All of the simulations were performed at a 16-node Linux cluster. Each node contains four Itanium II processors operating at 1.3 GHz.

4. Results

4.1. Liquid Densities. In the NPT ensemble, the liquid density can be obtained directly. As the literature suggested, the density data can be used to validate a proposed force field of the RTILs.[17] To confirm that equilibrium was indeed reached, the evolution of density for TMGL during the simulation run is shown in Figure 4. In this work, the simulation results are compared with experimental data in Table 6. The simulation densities are in good agreement with experimental results for TMGP and TMGT.

It is noticed that sometimes trace amounts of impurities such as water, chloride, and sodium ions in RTILs could change the value of the density dramatically.[17,30] The experimental data may be influenced by little water which is difficult to remove completely. For example, the experimental density for TMGL at 318 K in the literature is 1.07 g/cm^3,[6] and our experimental one is 1.13 g/cm^3. The purity of the sample in the literature[6] was not reported. In our laboratory, the TMGL sample was dried under vacuum at 373 K for 48 h and the measured water content was less than 200 ppm by using the 787 KF Titrino method (a titrator for water determination according to the Karl Fisher

TABLE 6: Change of Internal Energies for Vaporization, Intermolecular Energies, Interaction Energies of the Ion Pairs, Heat of Vaporization, Molar Volumes, and Cohesive Energy Densities

						ρ (g/cm^3)			
RTIL	T (K)	U^{vap} (kJ/mol)	U^{int} (kJ/mol)	$U^{ionpair}$ (kJ/mol)	ΔH^{vap} (kJ/mol)	MD	exp	V_m (cm^3/mol)	c (J/cm^3)
TMGF	373	89.55	−567.49	−477.94	92.65	1.14		141.41	633.27
	353	92.38	−570.32		95.31	1.15		140.18	659.01
TMGL	373	99.42	−553.20	−453.78	102.52	1.11		184.92	537.64
	333	106.44	−560.22		109.21	1.13		181.65	585.98
	318	110.29	−564.07		112.93	1.14	1.13[a]/1.07	180.05	612.55
	298	116.22	−570.00		118.70	1.15		178.49	651.14
TMGP	373	173.60	−535.83	−362.23	176.70	1.19		161.51	1074.86
	333	178.44	−540.67		181.21	1.21		158.84	1123.39
	318	181.55	−543.78		184.19	1.22	1.18	157.54	1152.42
TMGT	373	109.16	−530.96	−421.80	112.26	1.26		184.70	591.02
	333	112.50	−534.30		115.27	1.29		180.40	623.61
	318	114.40	−536.20		117.04	1.30	1.27	179.01	639.05
TMGTf	373	130.48[b]	−524.05[b]	−393.57	133.58[b]	1.40[b]		192.65[b]	677.30[b]
	333	133.33[b]	−526.90[b]		136.10[b]	1.42[b]		189.93[b]	701.98[b]
	318	134.33[b]	−527.90[b]		136.97[b]	1.43[b]	1.29	188.61[b]	712.22[b]
TMGTf	373	48.05[c]	−531.28[c]	−483.23	51.15[c]	1.42[c]		189.93[c]	252.98[c]
	333	54.86[c]	−538.09[c]		57.63[c]	1.44[c]		187.30[c]	292.90[c]
	318	58.58[c]	−541.81[c]		61.22[c]	1.45[c]	1.29	186.00[c]	314.94[c]

[a] Measured in our laboratory. [b] Molecular dynamics simulation results based on the force field in this work. [c] Molecular dynamics simulation results based on the force field in the literature.[18]

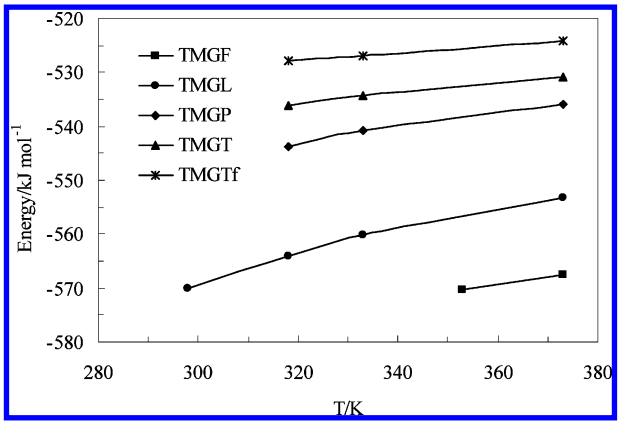

Figure 5. Total intermolecular energy.

method). Comparing the simulation density with our experimental result, the deviation is less than 1.0%.

The simulation densities are 1.43 and 1.45 g/cm^3 for TMGTf based on the force fields proposed by us and taken from the literature,[18] respectively. Both are relatively higher than the experimental value of 1.29 g/cm^3. One reason for the discrimination is that the anion force fields may not be sufficient to accurately represent the distribution of charges in the real systems; another crucial reason is that the LJ potential may not be realistic enough to describe interactions within these systems accurately, especially for hydrogen bonding.

4.2. Liquid Energy. The comparison between the electrostatic and LJ interactions for the five RTILs at 373 K is shown in Table 5. The total electrostatic interactions, which contribute to the major part of the total potential energy, are several times larger than the LJ interactions. It is clearly shown that the system energy is dominated by electrostatic interactions. It is also proved that the LJ interaction is dependent on the particle sizes by comparing the interaction energies of the cation and anion in each RTIL. The larger the particles size, the stronger the interaction will be.

The total intermolecular energies at different temperatures are shown in Table 6 and Figure 5. The intermolecular energies increase with increasing temperature for each RTIL. Generally, the sequence of the quantity for energy is TMGTf > TMGT > TMGP > TMGL > TMGF.

One of the most important properties of RTILs is their low vapor pressure, which can be studied by the heat of evaporation (ΔH^{vap}) and the cohesive energy density (c). They are defined as

$$\Delta H^{vap} = \Delta U^{vap} + RT \quad (2)$$

$$c = \Delta U^{vap}/V_m \quad (3)$$

R is the gas constant, and V_m is the molar volume of the liquid. The above equations are both related to ΔU^{vap}, which stands for the change of the internal energy after vaporization. It can be simplified by[11]

$$\Delta U^{vap} = U^{ionpair} - U^{int} \quad (4)$$

In Table 6, the changes of the internal energy for vaporization, intermolecular energies, interaction energies of the ion pairs, heat of vaporization, molar volumes, and cohesive energy densities at different temperatures are presented. In contrast, the cohesive energy densities of the heavy hydrocarbons and naphthalene are 268 and 410 J/cm^3, respectively.[8,31] The extremely high cohesive energy density of the five guanidinium-based RTILs explains why these liquids have such a low volatility.

4.3. Microstructure. The center-of-mass radial distribution functions (RDFs) are used to study the microstructure of the RTILs. The RDFs of the same RTIL at different temperatures are almost the same, and only the RDFs at 373 K for cation−cation, cation−anion, and anion−anion of the five RTILs are shown in Figure 6. Molten salts are characterized by strong oscillations in the radial distribution functions and are considered as strongly coupled ionic systems.[1,32] As can be seen in Figure 6, all of the oscillations extend beyond 16 Å, which is approximately the half-length of the simulation box, which is more evidence for electrostatic interactions being the major component of the system energy. Also, it can be seen in Figure 6 that there is one shoulder peak at 4.24 and 4.88 Å in $g(r)$ for TMGP and TMGTf, respectively, which may be due to the tendency of anions distributing above or below the TMG cation plane (refer to Figure 8).

The organization of the bulk liquid can also be analyzed in a condensed phase MD simulation by examining the coordina-

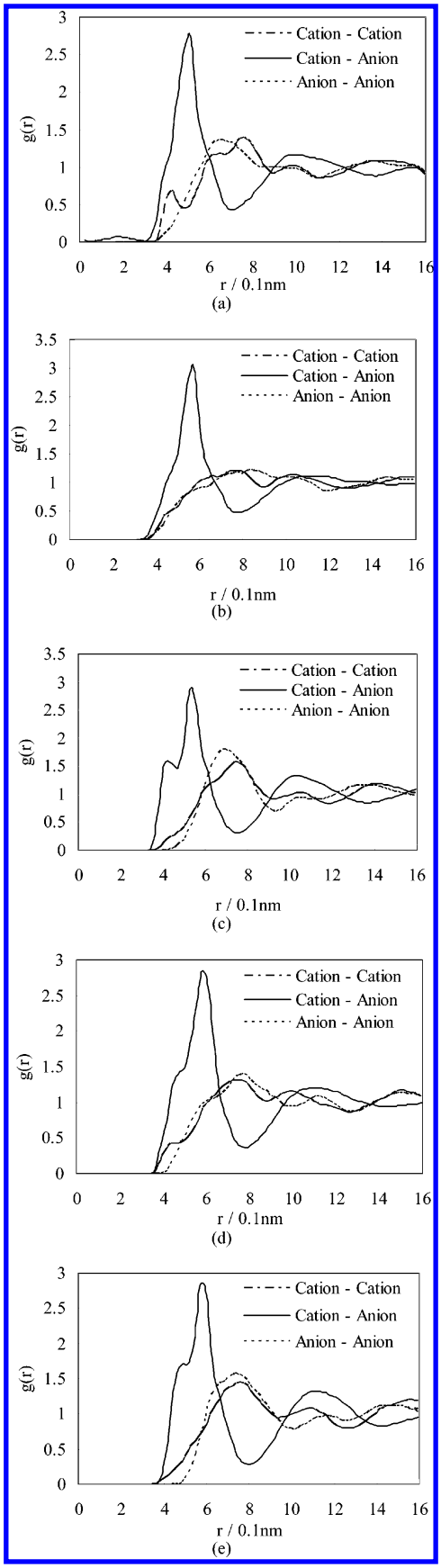

Figure 6. Center-of-mass radial distribution functions at 373 K: (a) TMGF; (b) TMGL; (c) TMGP; (d) TMGT; (e) TMGTf.

tion numbers via the integral of RDFs from zero to the first minimum, which is simply the average number of specific sites or atoms within a sphere of radius r about some other central

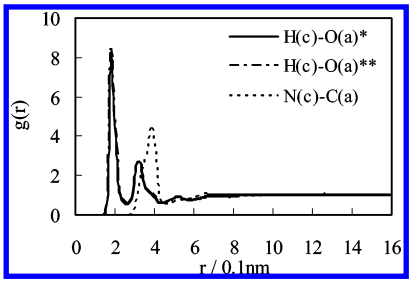

Figure 7. Site−site radial distribution functions for TMGL. c, cation; a, anion; *, oxygen atom near H1; **, oxygen atom near OH.

TABLE 7: First Solvation Shell of Center-of-Mass RDFs

RTIL	max position (Å)	min position (Å)	coordination no.
TMGF	5.04	7.12	7.2
TMGL	5.68	7.76	7.3
TMGP	5.36	7.44	7.1
TMGT	5.84	7.76	7.4
TMGTf	5.84	7.92	7.3

TABLE 8: Max and Min Positions of Site−Site RDFs and the First Shell Coordination Numbers

RTIL	T (K)	site−site	max position (Å)	min position (Å)	peak height	coordination no.
TMGF	373	H−O	1.84	2.66	7.05	0.53
	353	H−O	1.84	2.66	7.34	0.52
TMGL	373	H−O	1.80	2.60	8.17	0.54
	333	H−O	1.80	2.60	8.51	0.53
	318	H−O	1.80	2.60	8.69	0.53
	298	H−O	1.80	2.60	8.77	0.53
TMGP	373	H−O	1.99	2.66	2.36	0.28
	333	H−O	1.99	2.66	2.59	0.29
	318	H−O	1.99	2.66	2.68	0.29
TMGT	373	H−O	1.84	2.66	8.09	0.51
	333	H−O	1.84	2.66	8.55	0.50
	318	H−O	1.84	2.66	9.39	0.52
TMGTf	373	H−O	1.88	2.68	4.58	0.34
	333	H−O	1.88	2.68	5.08	0.34
	318	H−O	1.88	2.68	5.20	0.34

site or atom. The first solvation shell can be calculated by[17]

$$N = 4\pi \int_0^{\mathrm{Rmim1}} \rho g(r) r^2 \, \mathrm{d}r \qquad (5)$$

where ρ is the number density. The solvation shell locations and the coordination numbers for the five kinds of RTILs are listed in Table 7. It can be seen that each cation is surrounded by seven to eight anions no matter the difference of these RTILs. It is indicated that the cation plays the most important part in the structures of these guanidinium-based RTILs. Two solvation shells are found for all five RTILs within 16 Å. The cation−anion peaks are well-defined, sharper, and located at a shorter distance than the identical ion pairs.

Further insight into the liquid structures can be gained by examining the site−site pair RDFs. Take TMGL, for example, it could be found in Figure 7 that there are hydrogen bonds formed by the amino group in the cation and the oxygen atom of the carboxylic acid in the anion. The obvious higher peaks of the H−O RDFs explain the strong interactions of the hydrogen bonds. The RDFs for each oxygen atom of the carboxylic acid group with the cation seem indiscriminative. The site−site solvation shells were obtained via the integral of site−site RDFs using formula 5, and they are listed in Table 8. It is predicted that every hydrogen atom in the amide group forms a hydrogen bond at the same probability with any oxygen atom in the carboxylic acid group. The site−site locations of the solvation shells and coordination numbers of the five RTILs at different temperatures are also listed in Table 8. It can be

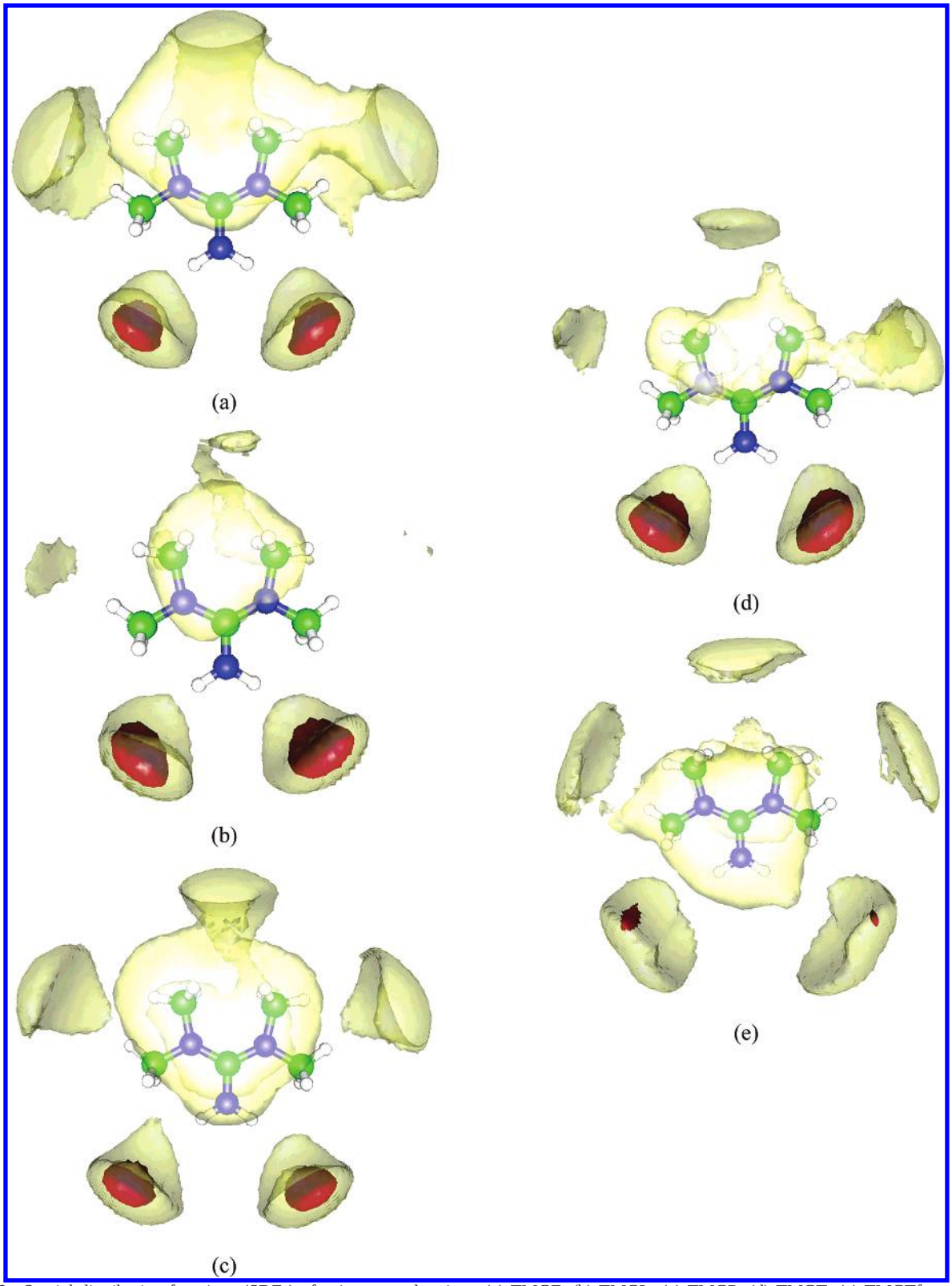

Figure 8. Spatial distribution functions (SDFs) of anion around cation: (a) TMGF; (b) TMGL; (c) TMGP; (d) TMGT; (e) TMGTf.

seen that the peak heights of these site−site RDFs become lower with increasing temperature.

To obtain more visual structures of these RTILs, the spatial distribution functions (SDFs) that stand for the three-dimensional probability distributions of anion and cation were studied. In this work, the SDFs are visualized by the software package gOpenMol.[33] The SDFs for anion around cation are shown in Figure 8. In each case, the coordinate lengths in the *x*, *y*, and *z* directions are chosen to be 30 Å, and the red and yellow contour surfaces are drawn at 20 and 4 times of the average density, respectively. From the O−H coordination number data in Table 8 and the SDFs in Figure 8, it can be understood that two anions locate next to the hydrogen atoms in the amino-group terminal and the other anions within the first solvation shell are most likely distributed above or below the plane or around the methyl. Since the nature of the major interactions between the cation

and anion is the same in all of the investigated cases, the smallest F anion also shows much the same distribution as the largest Tf anion.

The probability distributions of these anions around the cation are similar but with different characteristics. The anions most likely distribute next to the hydrogen atoms in the amino-group terminal, while the tendency for TMGTf is reduced compared with the others. The yellow region shifts above or below the plane as the anion changes from F to L, mainly due to the size of the anion.

5. Conclusions

In this work, the force field based on AMBER is proposed for a new class of *N*,*N*,*N*′,*N*′-tetramethylguanidinium-based ionic liquids. The refinement of the force field includes fitting the vibration frequency and torsion energy profiles in the frame of AMBER using a systematic way. Molecular dynamics simulations for five *N*,*N*,*N*′,*N*′-tetramethylguanidinium-based RTILs at different temperatures were performed to validate the proposed force field. The calculated liquid densities are consistent with the experimental results. The potential energies of the RTILs were studied. It is found that the ionic liquids have extremely high cohesive energy densities and heats of vaporization, which explain their very low vapor pressures. The microstructures are discussed by radial distribution functions (RDFs) and spatial distribution functions (SDFs). The amino groups in the cation form hydrogen bonds with each kind of anion. It is found that the two anions locate next to the hydrogen atoms in the amino-group terminal and the other anions within the first solvation shell most likely distribute above or below the plane or around the methyl. Finally, it is under progress to test the possibility of extending the present parametrization to other members of the guanidinium family.

Acknowledgment. The authors sincerely appreciate the helpful discussions with Prof. Wenchuan Wang and Dr. Zhiping Liu in Beijing University of Chemical Technology (BUCT) and financial support by National Natural Science Foundation of China (20436050).

References and Notes

(1) Del Po'polo, M. G.; Voth, G. A. *J. Phys. Chem. B* **2004**, *108*, 1744.
(2) Cole, A. C.; Jensen, J. L.; Ntai, I.; Tran, K. L. T.; Weaver, K. J.; Forbes, D. C.; Davis, J. H., Jr. *J. Am. Chem. Soc.* **2002**, *124*, 5962.
(3) Rajagopal, R.; Jarikote, A.; Dilip, V.; Srinivasan, K. V. *Chem. Commun.* **2002**, *67*, 616.
(4) Sheldon, R. *Chem. Commun.* **2001**, *66*, 2399.
(5) Blanchard, L. A.; Hancu, D.; Beckman, E. J.; Brennecke, J. F. *Nature* **1999**, *399*, 28.
(6) Gao, H.; Han, B.; Li, J.; Jiang, T.; Liu, Z.; Wu, W.; Chang, Y.; Zhang, J. *Synth. Commun.* **2004**, *34*, 3083.
(7) Margulis, C. J.; Stern, H. A.; Berne, B. J. *J. Phys. Chem. B* **2002**, *106*, 12017.
(8) Morrow, T. I.; Maginn, E. J. *J. Phys. Chem. B* **2002**, *106*, 12807.
(9) Wang, P.; Zakeeruddin, S. M.; Grätzel, M.; Kantlehner, W.; Mezger, J.; Stoyanov, E. V.; Scherr, O. *Appl. Phys. A* **2004**, *79*, 73.
(10) Welton, T. *Chem. Rev.* **1999**, *99*, 2071.
(11) Wasserscheid, P.; Keim, W. *Angew. Chem., Int. Ed.* **2000**, *39*, 3773.
(12) Sheldon, R. *Chem. Commun.* **2001**, 2399.
(13) Dupont, J.; De Souza, R. F.; Suarez, P. A. Z. *Chem. Rev.* **2002**, *102*, 3667.
(14) Zhang, S.; Yuan, X.; Chen, Y.; Zhang, X. *J. Chem. Eng. Data* **2005**, *50*, 1582.
(15) Xie, H.; Zhang, S.; Duan, H. *Tetrahedron Lett.* **2004**, *45*, 2013.
(16) MacKerell, A. D.; Bashford, D.; Bellott, M.; Dunbrack, R. L.; Evanseck, J. D.; Field, M. J.; Fischer, S.; Gao, J.; Guo, H.; Ha, S.; Joseph-McCarthy, D.; Kuchnir, L.; Kuczera, K.; Lau, F. T. K.; Mattos, C.; Michnick, S.; Ngo, T.; Nguyen, D. T.; Prodhom, B.; Reiher, W. E.; Roux, B.; Schlenkrich, M.; Smith, J. C.; Stote, R.; Straub, J.; Watanabe, M.; Wiorkiewicz-Kuczera, J.; Yin, D.; Karplus, M. *J. Phys. Chem. B* **1998**, *102*, 3586.
(17) Liu, Z.; Huang, S.; Wang, W. *J. Phys. Chem. B* **2004**, *108*, 12978.
(18) Lopes, J. N. C.; Pádua, A. A. H. *J. Phys. Chem. B* **2004**, *108*, 16893.
(19) Criado, A.; Diánez, M. J.; Pérez-Garrido, S.; Fernandes, I. M. L.; Belsley, M.; de Matos Gomes, E. *Acta Crystallogr.* **2000**, *56*, 888.
(20) de Andrade, J.; Boes, E. S.; Stassen, H. *J. Phys. Chem. B* **2002**, *106*, 13344.
(21) Pappu, R. V.; Hart, R. K.; Ponder, J. W. *J. Phys. Chem. B* **1998**, *102*, 9725.
(22) Lii, J. H.; Allinger, N. L. *J. Am. Chem. Soc.* **1989**, *111*, 8566.
(23) Cornell, W. D.; Cieplak, P.; Bayly, C. I.; Gould, I. R.; Merz, K. M.; Ferguson, D. M.; Spellmeyer, D. C.; Fox, T.; Caldwell, J. W.; Kollman, P. A. *J. Am. Chem. Soc.* **1995**, *117*, 5179.
(24) Fox, T.; Kollman, P. A. *J. Phys. Chem. B* **1998**, *102*, 8070.
(25) Cornell, W. D.; Cieplak, P.; Bayly, C. I.; Kollman, P. A. *J. Am. Chem. Soc.* **1993**, *115*, 9620.
(26) Cieplak, P.; Cornell, W. D.; Bayly, C.; Kollman, P. A. *J. Comput. Chem.* **1995**, *16*, 1357.
(27) Wang, J. M.; Cieplak, P.; Kollman, P. A. *J. Comput. Chem.* **2000**, *21*, 1049.
(28) Lyubartsev, A. P.; Laaksonen, A. *Comput. Phys. Commun.* **2000**, *128*, 565.
(29) Martyna, G. J.; Tuckerman, M. E.; Tobias, D. J.; Klein, M. L. *Mol. Phys.* **1996**, *87*, 1117.
(30) Wang, J. J.; Tian, Y.; Zhao, Y.; Zhuo, K. *Green Chem.* **2003**, *5*, 618.
(31) Hildebrand, J. H.; Scott, R. L. *Regular Solutions*; Prentice Hall: Englewood Cliffs, NJ, 1962.
(32) Keblinshi, P.; Eggebrecht, J.; Woff, D.; Phillpot, S. R. *J. Chem. Phys.* **2000**, *113*, 282.
(33) Laaksonen, L. *J. Mol. Graphics* **1992**, *10*, 33.